Experimental Investigation of Highly Separated Transitional Shockwave Boundary Layer Interactions

Theodor-Andrei DRAGHICI*,[1,2], Ferdinand SCHRIJER[3], Bas van OUDHEUSDEN[3]

*Corresponding author
[1]Structures and Materials Department,
INCAS – National Institute for Aerospace Research "Elie Carafoli",
B-dul Iuliu Maniu 220, Bucharest 061126, Romania,
draghici.andrei@incas.ro*
[2]Faculty of Aerospace Engineering,
National University of Science and Technology "Politehnica" Bucharest, Romania,
Gheorghe Polizu 1, 011061, Bucharest, Romania
[3]Faculty of Aerospace Engineering,
Delft University of Technology, Delft, Netherlands,
F.F.J.Schrijer@tudelft.nl, B.W.vanOudheusden@tudelft.nl

DOI: 10.13111/2066-8201.2025.17.4.5

Received: 15 September 2025/ Accepted: 22 October 2025/ Published: December 2025

Abstract: *Oblique shock wave - boundary layer interactions (OSBLIs) at transitional Reynolds numbers are known to generate low-frequency unsteadiness that can impact aerodynamic efficiency, structural integrity, and system reliability in high-speed aerospace components. The present research examines how variations in Mach number, Reynolds number, and inviscid pressure jump influence the dynamics of these transitional interactions. Experimental campaigns were conducted in the TST-27 transonic–supersonic wind tunnel at TU Delft, utilizing high-speed and spark-light Schlieren imaging to capture flow behavior, followed by digital and spectral post-processing. The results reveal that transitional OSBLIs exhibit low-frequency shock oscillations strongly correlated with the periodic formation and disappearance of a Mach stem, a mechanism referred to as the "dual-domain" phenomenon. Systematic parameter variations showed that even small changes in Mach or Reynolds number substantially altered the presence of this dual domain as well as the amplitude and frequency of the oscillations. Furthermore, the Reynolds number regime previously identified as transitional for flat-plate boundary layers was experimentally validated in the present configuration. A secondary focus of the study was the application of passive flow control by introducing thin two-dimensional steps (≈60 μm) to trip the boundary layer. These perturbations were found to effectively suppress shock oscillations and modify the overall interaction dynamics, with frequency analyses confirming the disappearance of oscillation peaks observed in the baseline cases. A nondimensional analysis demonstrated a consistent Strouhal number convergence around St ≈ 0.33 for cases with strong unsteadiness. Increasing Reynolds number led to reduced laminar separation lengths and higher oscillation frequencies, consistent with expected transition dynamics. Overall, this research identifies the primary parameters governing unsteadiness in transitional OSBLIs, highlights effective suppression through minimal boundary-layer tripping, and provides nondimensional scaling to support predictive modeling. These insights contribute to improved understanding and design of aerospace components subject to shock-induced boundary-layer interactions.*

Key Words: *shockwave-boundary layer interactions, low-frequency unsteadiness, shock oscillations, passive flow control, digital processing*

1. INTRODUCTION

Shock wave - boundary layer interactions (SBLIs) represent a fundamental challenge in high-speed aerodynamics due to their impact on both performance and structural integrity. When a shock wave impinges on a surface boundary layer, the resulting interaction can lead to boundary-layer separation, shock unsteadiness, and high thermal and mechanical loads [1].

Historical flight tests with the North American X-15 highlighted the severity of these effects [2]. At Mach 6.7, shock interactions around the supporting pylon of a "dummy scramjet" produced extreme local heating, leading to structural failure of the panel and loss of the test article in flight (Figure 1a).

Similarly, "blunt-fin" SBLIs around protruding components such as ultra-high frequency (UHF) antennas have been shown to generate severe aerothermal heating and material degradation (Figure 1b) [2]. These examples show that SBLIs are not only a matter of aerodynamic efficiency but also a limiting factor for the durability and safety of high-speed flight systems.

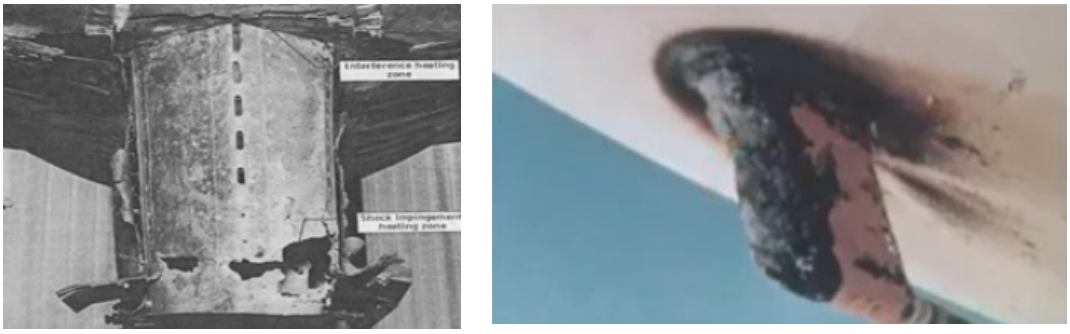

a) front view of the panel holding the dummy pylon

b) aerothermal heating of UHF Antenna (blunt fin SBLI)

Figure 1. Outcome of the SBLI for components of the X-15 during flight at M = 6.7 [2]

A schematic representation of an oblique shock–boundary layer interaction (OSBLI) is shown in Figure 2.

When an oblique shock impinges on the boundary layer, the flow typically separates upstream of the shock, creating a recirculation region that generates compression waves and modifies the reflected shock structure [1].

The separated bubble ends with a reattachment shock, while an expansion fan forms as the separated shear layer "relaxes" downstream. Such mechanisms are characteristic of OSBLIs in transonic and supersonic flows, where SBLIs can lead to separation, drag increase, and flow unsteadiness.

These effects are of particular importance in applications such as supersonic intakes, compressors, and turbines, where uncontrolled OSBLIs may compromise efficiency and stability, or even lead to mechanical failure [1].

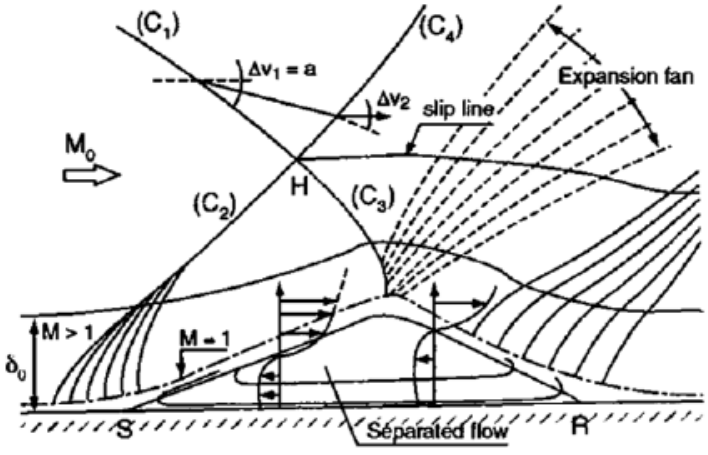

Figure 2. Schematic of an Oblique SBLI [1]

In transonic compressor and fan flows, the passage shock can exhibit strong unsteady behavior that is closely linked to oblique shock–boundary layer interactions. Doerffer et al. [3] and Nel et al. [4] identify three main regimes:

- Detached shock with subsonic flow: a bow shock forms ahead of the leading edge, creating directly subsonic flow after the shock. This leads to minimal flow separation. The bow shock will likely oscillate around the leading edge, indicating an unsteady behavior.
- Lambda passage shock: by reducing the back pressure, a supersonic leading edge shockwave forms, which remains steady. This scenario is characterized by significant flow separation and is the primary case of interest.
- Swallowed passage shock: a further reduction in back pressure results in a smaller separation compared to the lambda passage shock case.

Denton [5] further illustrated these mechanisms by describing typical shock structures near compressor blade tips, emphasizing their role in driving local separation and unsteadiness. Of the three regimes, the lambda configuration is of primary interest, as it induces large-scale separation and oscillatory shock behavior. At low Reynolds numbers, such as those encountered in the high-altitude operation of business jets and military aircraft [6], the boundary layer approaching the shock may remain laminar, which increases the likelihood of separation-driven instabilities.

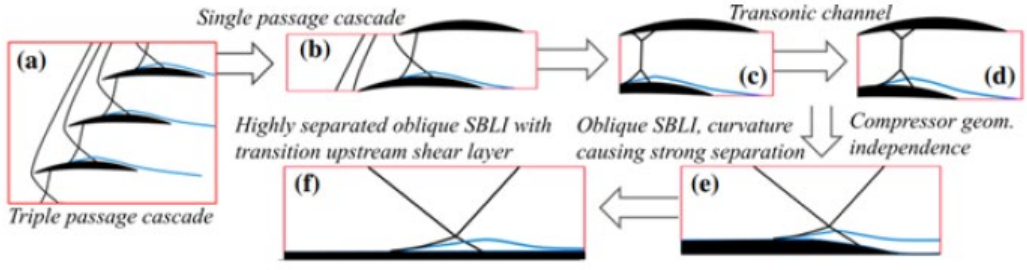

Figure 3. Simplification of the low Reynolds transonic fan shock oscillation problem to the most fundamental form [4]

Nel et al. [4], [6], [7] demonstrated that the passage shock dynamics in these conditions are analogous to laminar OSBLIs on flat plates: the unsteadiness is governed by the periodic growth and collapse of a separation bubble, which drives a “breathing” motion of the shock

system. This cycle is associated with Kelvin–Helmholtz instabilities in the separated shear layer and, in some cases, with the intermittent appearance of a Mach stem, further contributing to low-frequency content in the shock oscillations. These findings are illustrated in Figure 3.

Shock wave - boundary layer interactions (SBLIs) arise when the adverse pressure gradient imposed by a shock wave interacts with the low-momentum fluid near the wall. The boundary layer may thicken, separate, or even reverse, giving rise to unsteadiness and large-scale flow instabilities. These mechanisms are critical in transonic and supersonic regimes, where SBLIs can drive phenomena such as wing buffeting, intake buzz, or unsteady nozzle side loads, ultimately limiting aerodynamic performance and structural integrity [1].

A convenient framework for describing these interactions is the so-called boundary-layer – shock - pressure-jump competition introduced by Babinsky & Harvey [1]. Starting from the streamwise momentum equation for the boundary layer,

$$\rho u \frac{\partial u}{\partial x} + \rho v \frac{\partial u}{\partial y} = -\frac{dp}{dx} + \frac{\partial \tau}{\partial y} \tag{1}$$

it becomes clear that the shock-induced adverse pressure gradient "competes" against the shear stress within the boundary layer. If the low-speed near-wall flow cannot provide sufficient shear to counter the imposed pressure rise, separation occurs. Figure 4 illustrates this balance of forces, where momentum transfer from the outer high-speed layers sustains the inner shear against the pressure rise until a critical threshold is reached.

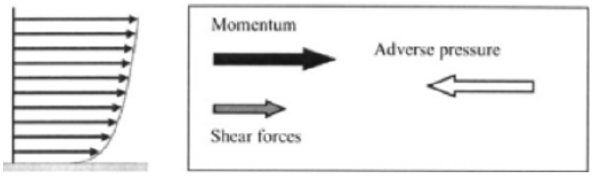

Figure 4. Acting forces in an SBLI [1]

For clarity, the equation can be simplified by neglecting the wall-normal velocity and treating the boundary layer as a parallel flow, leading to:

$$\frac{d}{dx}\int_{\delta_i}^{\delta} \rho u^2 \, dy \approx -\frac{dp}{dx}(\delta - \delta_i) + \left(\tau_\delta - \tau_{\delta_i}\right) \approx -\frac{dp}{dx}\delta \tag{2}$$

where δ_i is an "inner" boundary layer thickness. The simplified equation above shows the relationship between the flow momentum and the pressure gradient. Laminar and transitional (within the scope of the present paper) boundary layers have profiles and characteristics that may not withstand a strong pressure gradient coming from a shockwave, making boundary-layer separation – and hence unsteadiness – more pronounced.

An additional framework frequently applied to shock - boundary layer interactions is the *free interaction theory* developed by Chapman [8]. The central hypothesis is that the upstream flow development prior to the shock impingement is largely independent of the shock generator or its specific strength, provided that the inviscid pressure jump, Mach number, and boundary-layer state remain similar. A widely used formulation for laminar or transitional interactions, adapted from Erdos and Pallone [9], expresses the pressure rise in terms of a correlation function:

$$C_p(\bar{x}) = F(\bar{x}) \sqrt{\frac{2C_{f0}}{\sqrt{Ma^2 - 1}}} \tag{3}$$

where $\bar{x} = (x - x_{sep})/L_{sep}$ denotes the normalized streamwise coordinate relative to the separation point. This relation links the pressure development in the onset region of the interaction directly to upstream boundary-layer conditions. Experimental studies, such as those by Giepman [10], demonstrated that varying the shock impingement angle within a certain range produced nearly identical upstream pressure distributions, confirming that the essential source of unsteadiness lies in the interaction process itself rather than in the precise shock geometry.

2. THE UNSTEADINESS OF SBLIS

The unsteady nature of shock wave–boundary layer interactions has been widely studied, as these oscillations can drive severe aerodynamic and structural consequences [11]. A systematic comparison of different SBLI configurations—including oblique interactions, compression ramps, blunt fins, and nozzle flows—was made by Dussauge et al. [12]. Their results highlighted that the characteristic unsteadiness could be scaled using the nondimensional excursion length, defined as L_{ex}/L, where $L_{ex}$is the distance travelled by the reflected shock during one oscillation cycle and L, the characteristic interaction length. Across a wide range of configurations, this value consistently fell between 0.3 and 0.5, reinforcing the idea that the interaction length Las the appropriate scaling parameter for Strouhal number analyses (Figure 5a).

This finding provides a universal framework for comparing unsteadiness across different Mach numbers, geometries, and flow conditions.

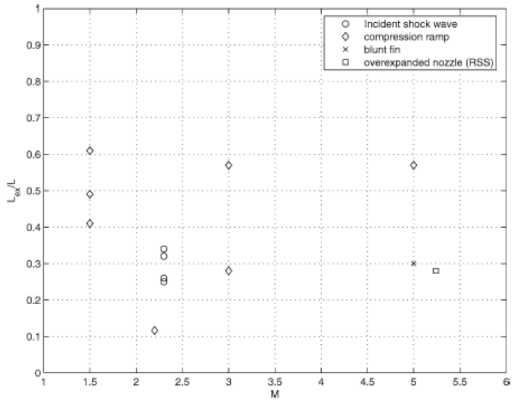

a) Oscillation length for the unsteady shock for different configurations

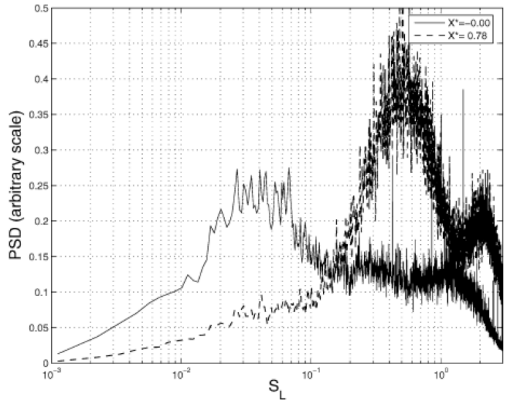

b) Power spectral density of wall pressure fluctuations – comparison between the "foot" of the reflected shock and the interaction zone

Figure 5. Main parameters driving the unsteadiness of OSBLIs [12]

Further spectral analyses of wall-pressure fluctuations further demonstrated the distinct frequency content associated with different regions of the interaction [12]. At the shock foot, where the reflected shock attaches to the surface, the spectrum is dominated by a low-frequency peak.

Further inside the interaction zone, higher frequencies are recorded, consistent with the dynamics of the separated shear layer (Figure 5b). This distinction emphasizes the multi-scale nature of SBLI unsteadiness.

3. SHOCK-SHOCK INTERACTIONS AND SHOCK POLARS

When a boundary layer separates in the presence of an impinging shock, at least two shocks coexist: the original impinging shock and a separation shock generated by the effective "ramp" formed at the detachment point. Their interaction produces a combined shock system that can be classified using shock polar analysis. Shock polars, based on the Rankine–Hugoniot relations, provide a graphical framework for linking flow deflection angle to the pressure rise across the shock. For a given Mach number and deflection angle, the weak and strong solutions can be identified, highlighting the downstream pressure and Mach states. The pressure ratio across an oblique shock can be expressed as:

$$\frac{p}{p_1} = \left[\frac{(\gamma+1)Ma^2\sin^2\beta}{(\gamma-1)Ma^2\sin^2\beta+2}\right]^{\frac{\gamma}{\gamma-1}} \left[\frac{\gamma+1}{2\gamma Ma^2\sin^2\beta-(\gamma-1)}\right]^{\frac{1}{\gamma-1}} \tag{4}$$

where M_a is the upstream Mach number, β the shock angle, and γ the ratio of specific heats. Two distinct regimes can be identified depending on shock strength. In Type I shock–shock interference (Figure 6a and Figure 6c), corresponding to a regular reflection, the impinging and separation shocks intersect on the shock polar plane, resulting in a single slip line. This configuration is typical of weaker interactions. By contrast, in Type II interference (Figure 6b and Figure 6d), the curves no longer intersect, leading to the formation of a Mach stem and two slip lines, an indicator of a stronger interaction [1], [13]. These polar-based interpretations clarify how the separation bubble modifies the local flow angles and pressures, and they can be used to see whether a regular reflection or a Mach reflection appears during the intersection of the impinging shockwave and the separation shockwave.

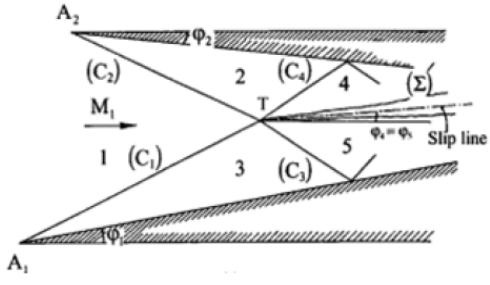

a) Type I shock-shock interference

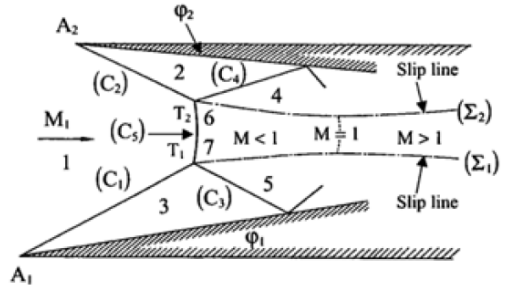

b) Type II shock-shock interference

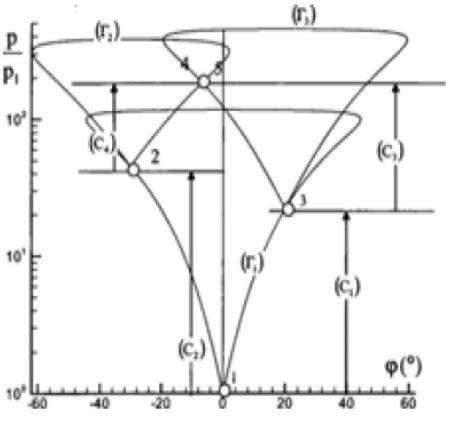

c) Type I shock-shock interference polar plane

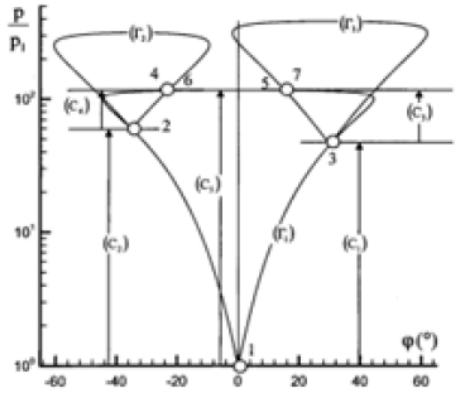

d) Type II shock-shock interference polar plane

Figure 6. Types of shock-shock interferences encountered in SBLIs [1]

4. TRANSITIONAL OSBLIS

Transitional shock–boundary layer interactions represent a "hybrid" flow regime that combines features of both laminar and turbulent SBLIs. The defining characteristic of these cases is that the boundary layer remains laminar at the onset of separation but undergoes rapid transition under the influence of shock-induced instabilities. This transition alters the separation dynamics and modifies the overall structure of the interaction, producing distinct unsteady features that are not present in purely laminar or turbulent cases [14], [15].

High-speed and spark-light Schlieren visualizations from experiments in the TST-27 facility at TU Delft provide direct evidence of such mechanisms (Figure 7). As the separation shockwave moves upstream, the laminar boundary layer transitions earlier than in the natural case, generating a fan of compression waves that coalesce into a turbulent separation shock. The result is an interaction structure that departs from the classical single-shock schematic, as additional compression and reattachment occur downstream [6]. This accelerated transition mechanism demonstrates that the presence of even a weak oblique shock can significantly shift the stability characteristics of the incoming boundary layer.

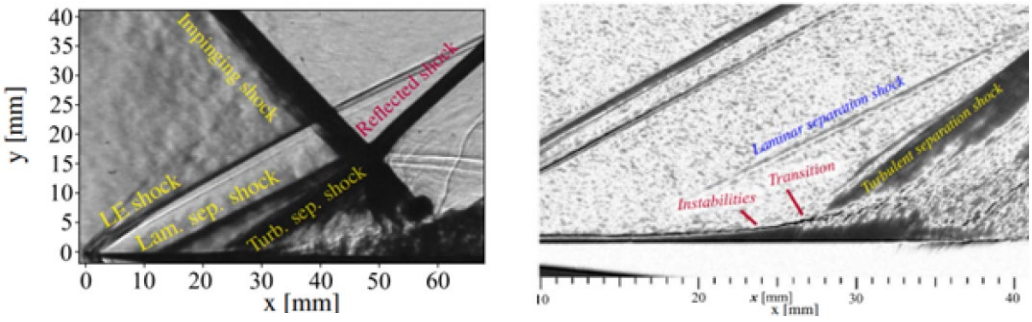

a) High speed Schlieren visualization b) Spark light Schlieren visualization

Figure 7. Transitional OSBLI physical phenomenon [6]

Despite these observations, the precise causes of shock oscillations in transitional OSBLIs remain uncertain. Some experiments display strong low-frequency unsteadiness, while others under comparable conditions do not. This variability underscores the need to determine the Reynolds-number range over which the boundary layer is transitional, and how its state couples with the separation bubble dynamics. As highlighted by Giepman [10], careful characterization of transition location and progression is essential for linking the observed oscillatory shock behavior to the underlying boundary-layer physics.

5. EXPERIMENTAL DESIGN

The experiments were done in the TST-27 transonic–supersonic blowdown wind tunnel at TU Delft (Figure 8a). The facility operates from an external pressurized reservoir with supply pressures between 25 and 40 bar, delivering a Mach number range of 0.5–0.85 in the transonic regime and 1.15–4.2 for supersonic flows.

The test section measures 270 × 280 mm and includes optical access for flow visualization. Freestream conditions were derived from isentropic flow relations and Sutherland's law, with a nominal total temperature of 288 K. Schlieren visualizations in a Z-type configuration were used throughout to capture the shock dynamics, boundary-layer separation, and reattachment structures.

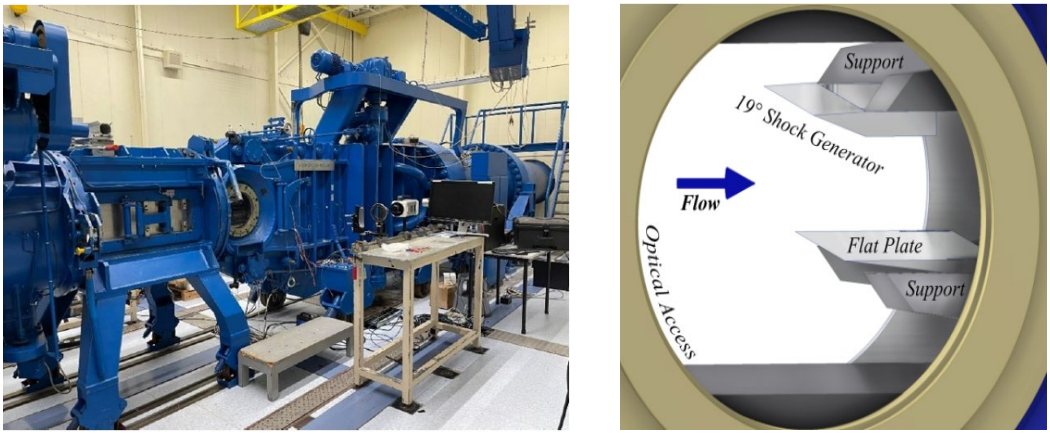

a) The TST 27 blowdown wind tunnel b) Shock generator and flat plate setup [6]

Figure 8. Experimental setup at the TU Delft facility

The test model consisted of a flat plate mounted parallel to the tunnel floor and a shock generator installed at the sidewall, replicating the configuration of previous OSBLI studies (Figure 8b). A detailed view of the geometry, including the 19° wedge and the flat plate, is provided in Figure 9.

This geometry was fixed across all tests to avoid tunnel unstart, which would occur if the wedge were positioned lower. The optical windows enabled Schlieren access for detailed recordings of the interaction region.

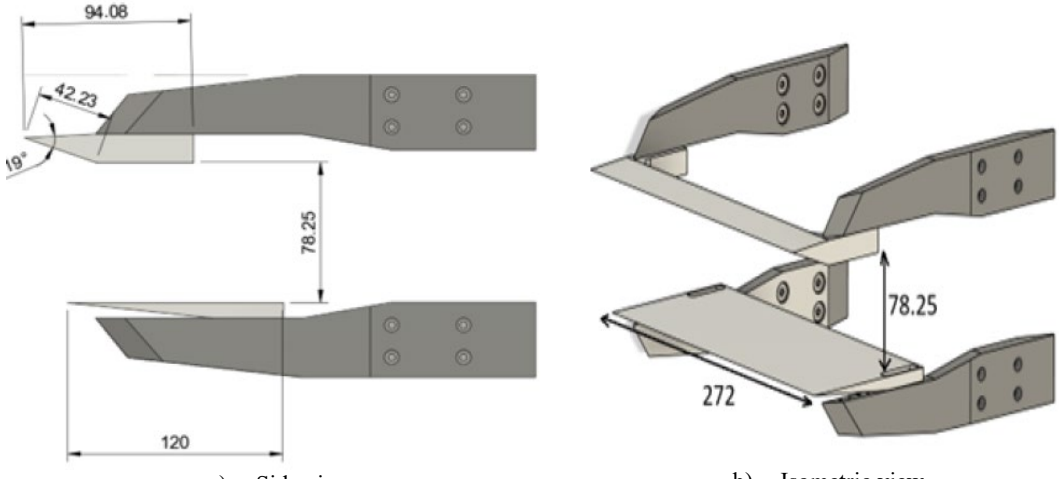

a) Side view b) Isometric view

Figure 9. Dimensions of the wind tunnel model with the 19º shock generator

To investigate passive flow control, a two-dimensional step was introduced on the flat plate surface using thin aluminum tape (Figure 10). Each layer provided a 60 μm step height, with strips cut to 1.3 mm width and positioned 3 mm downstream of the leading edge. This placement was chosen to influence the early stages of boundary-layer development and to remain effective across a range of Mach numbers, where the separation shock can move closer to the plate leading edge. Additional layers allowed step heights to be increased in 60 μm increments.

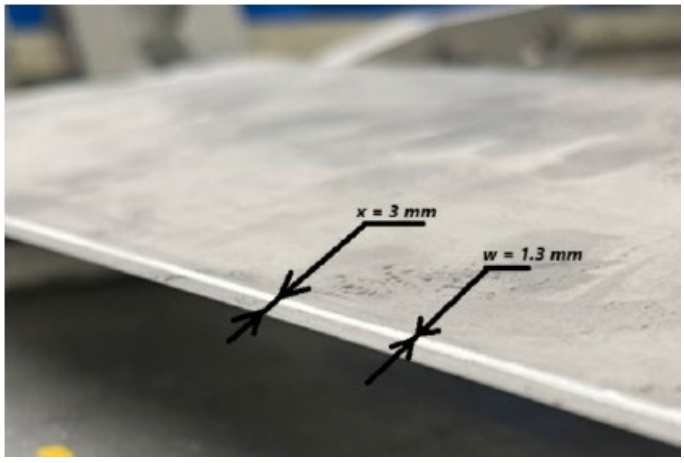

Figure 10. One layer (60 microns) of 2D step added to the flat plate

6. FLOW MEASUREMENT AND POST-PROCESSING TECHNIQUES

Schlieren visualizations were used to capture the shock–boundary layer interactions during the experiments, using a Z-type optical arrangement that works by identifying the refractive index gradients caused by the density variations in the flow. This technique makes shocks, expansion fans, and separation regions directly visible as sharp intensity changes in the recorded frames. The post-processing of these recordings began with the construction of mean and standard deviation images from the raw sequences. The mean image (Figure 11a) represents the time-averaged flow field, highlighting stationary features such as the average positions of the separation and reflected shocks. The standard deviation image (Figure 11b) shows regions of strong temporal variability, identifying zones of unsteadiness associated with the oscillating separation shock, the transitional region, and particularly the reflected shock, which displayed the highest intensity. Together, these complementary images provide both a static and dynamic overview of the flow, forming the basis for subsequent quantitative analyses.

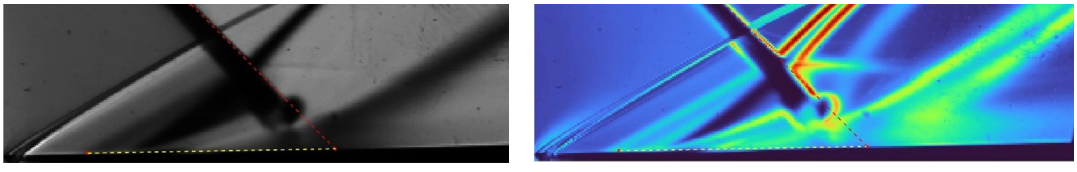

a) mean image b) standard deviation

Figure 11. Mean and standard deviation images of a test case: Ma = 2.3, pT = 2.8 bar

To further isolate the dominant time scales of the interaction, Fast Fourier Transform (FFT) and Power Spectral Density (PSD) analyses were applied to pixel intensity variations along selected lines crossing the key flow structures (Figure 12). By tracking the largest gradients across successive frames, time-series signals were extracted and processed using Welch's method, which applies Hamming windowing with 50% overlap to improve statistical convergence. This approach enabled the identification of low-frequency oscillations associated with the breathing of the separation bubble, as well as higher-frequency content linked to shear-layer instabilities, providing a spectral decomposition of the unsteady flow.

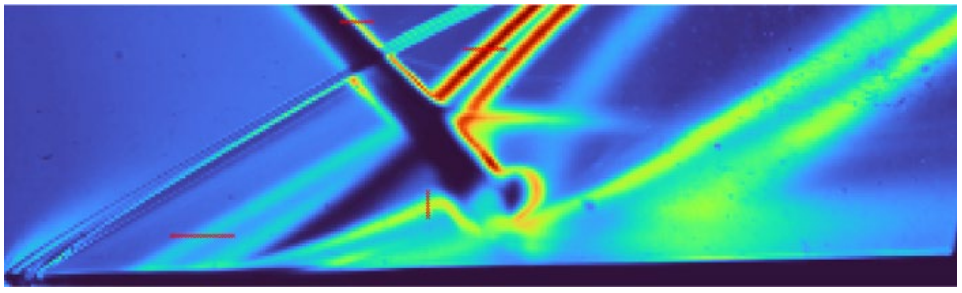

Figure 12. Locations where the FFT can be taken in the frequency analysis, test case Ma = 2.3, pT = 2.8 bar, 19º shock generator

Finally, a shock polar analysis (as described in the previous section) was used to interpret the observed oscillation mechanisms. Using flow parameters derived from the Schlieren recordings, the shock polars were constructed for the impinging and separation shocks, and their intersections were analyzed (Figure 13b).

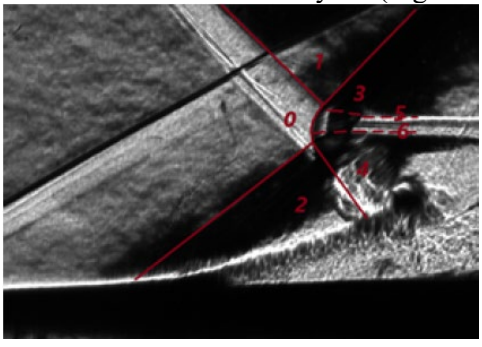

a) Spark light Schlieren image of the test

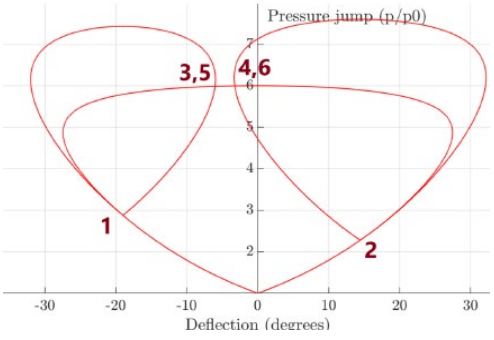

b) Shock polar extracted using the information from a)

Figure 13. Example of a shock polar analysis, test case Ma= 2.3, pT = 2.8 bar, 19º shock generator

As explained in Section 3, regular reflections correspond to intersecting polars, while the absence of an intersection indicates the formation of a Mach stem. What was interesting to notice during this post-processing was whether the appearance and the disappearance of the Mach stem would occur (which could be linked to the instability of the analyzed OSBLIs). This combined methodology, which used Schlieren visualization, statistical image processing, spectral analysis, and shock polar interpretation, offered a comprehensive framework to link the flow recordings with the underlying physics of transitional OSBLIs.

7. RESULTS

A large number of test cases were acquired during the campaign, requiring careful preselection to ensure a focused analysis. The final dataset (Table 1) was chosen based on several criteria: inclusion of all cases where the "desired" oscillation mechanism was observed; a grouping of tests that allowed a direct Reynolds number comparison; and the selection of cases where small changes in Mach number or shock generator angle produced completely different flow responses (see the "Observation" column in Table 1). In addition, tests at identical flow conditions but with varying shock generator angles were saved to assess the geometric sensitivity, while cases within the theoretical transitional Reynolds-number range were included to identify conditions where no laminar/transitional features were visible. The runs that led to a tunnel unstart were excluded. This filtering produced a representative set of

interactions, enabling systematic study of the parameters governing the investigated transitional OSBLIs.

Table 1. Tests selected for post-processing

No.	*Ma*	p_T [bar]	Re_x ($\cdot 10^6$)	Θ	Observation	Inviscid pressure rise
1	2.3	2.6	2.008	19°	Low oscillation amplitude	2.878
2	2.3	2.8	2.056	19°	Desired oscillation	2.878
3	2.3	4	2.968	19°	Low oscillation amplitude	2.878
4	2.3	4.2	3.228	19°	Very low oscillation amplitude	2.878
5	2.4	2.8	2.183	19°	Low oscillation amplitude	2.96
6	2.6	3.2	2.643	19°	Very low oscillation amplitude	3.143
7	2.6	3.4	2.792	19°	Very low oscillation amplitude	3.143
8	2.3	2.6	2.217	17°	Desired oscillation	2.6
9	2.4	2.8	2.48	17°	Low oscillation amplitude	2.6
10	2.4	2.8	1.896	22°	Desired oscillation	3.45
11	2.6	3.4	2.414	22°	Low oscillation amplitude	3.67
12	2.7	3.6	1.781	22°	Very low oscillation amplitude	3.79
13	2.7	3.8	1.814	22°	Very low oscillation amplitude	3.79

Referring to the previous paragraph, it is important to specify what is meant by the "desired" oscillation mechanism. The oscillation dynamics observed in the baseline case (Ma = 2.3, $p_T = 2.8$bar, 19° shock generator) are shown in Figure 14. The mechanism is cyclic: a laminar separation shock first forms and begins to propagate upstream (Figure 14a-c), followed by the growth of compression waves that form into a reflected shock, and ending with the "vanishing" of the propagating laminar separation shockwave as the OSBLI transitions (Figure 14d), which leads to a repeat of the process. The fading trace of a previous oscillation is often still visible while the next cycle begins, illustrating the quasi-periodic nature of the process. The timescales captured from consecutive Schlieren frames confirm that the shock system evolves on a low-frequency scale, consistent with the breathing motion of the separation bubble.

a) "initial state" – no upstream moving separation shock

b) 5 frames (0.063 ms) later

c) 19 frames (0.24 ms) later

d) 12 frames (0.15 ms) later

Figure 14. Description of the oscillation dynamics

A comparison of high-speed and spark-light Schlieren images (Figure 15) highlights the main flow structures that define this oscillation. Both visualizations clearly reveal the separation and reflected shocks, the transitional region linking the laminar and turbulent portions of the interaction, and the wedge-generated leading-edge shock. Together, these observations provide a direct experimental confirmation of the transitional OSBLI topology previously shown in schematic models, and they form the foundation for the subsequent frequency and Strouhal scaling analyses.

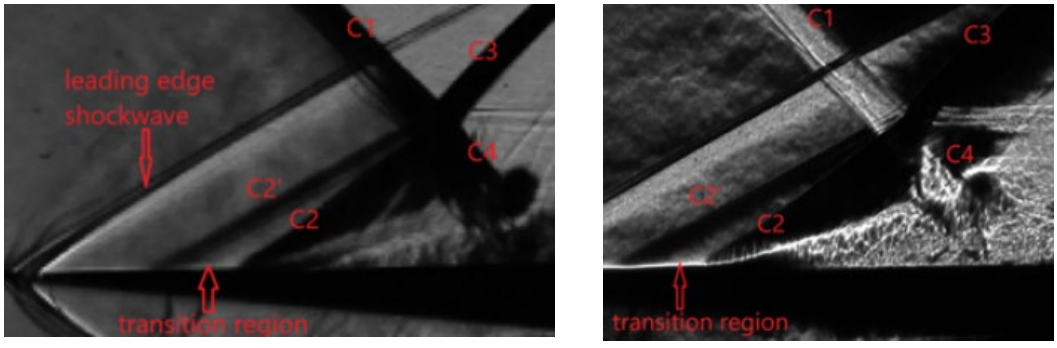

a) High speed Schlieren frame b) Spark light Schlieren frame

Figure 15. Topology of the components observed in the tests

Analysis of the baseline case with a desired oscillation: Ma = 2.3, pT = 2.8 bar, 19º s.g.

The baseline case, defined by the parameters $M_a = 2.3$, $p_T = 2.8\,\text{bar}$, and a 19° shock generator, serves as the reference for the analysis. This configuration had previously been shown by Nel et al. [4] to produce a dominant oscillation at ~3728 Hz, which was confirmed in the present study. Power spectral density (PSD) analysis of different regions of the interaction (separation shock, reflected shock, shear layer, impinging shock) demonstrated that the main elements of the system oscillated at the same frequency, consistent with the breathing motion of the separation bubble. In addition, a secondary low-frequency component (~100 Hz) was observed (Figure 16). Since this feature did not appear in freestream FFT analyses, it was attributed to mechanical vibration of the shock generator rather than an intrinsic flow instability.

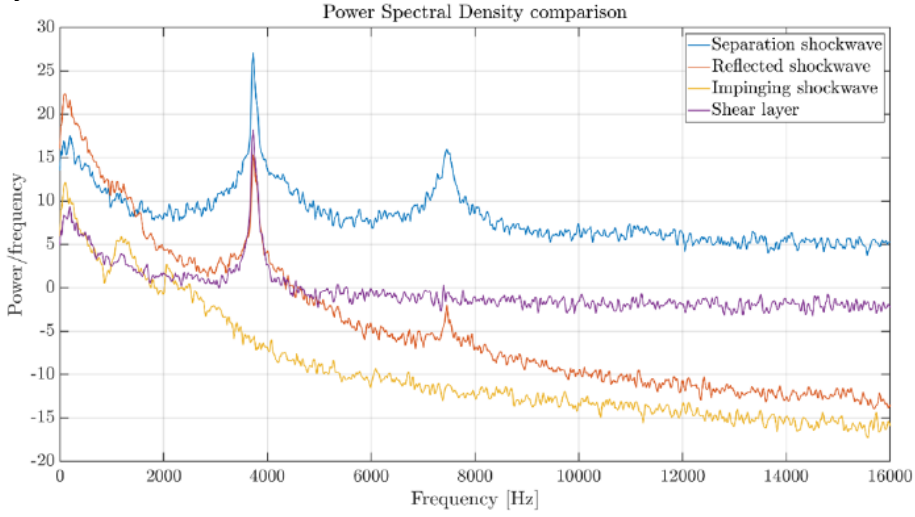

Figure 16. Power Spectral Density comparison between different regions of the flow for the baseline case

The Reynolds number for this case, calculated at the impingement point following Giepman's methodology [10], was $Re_x = 2.056 \times 10^6$, placing the interaction within the transitional regime. Within this framework, Schlieren visualizations revealed alternating phases of regular and Mach reflections. Angle measurements confirmed the distinction: when the separation shock angle was approximately 34°, the shock polars intersected, yielding a single slip line and thus a regular reflection (Figure 17a,b). Conversely, when the separation shock reached its most upstream position, the measured angle increased to ~38°, and the shock polars no longer intersected, producing two slip lines and confirming the presence of a Mach stem (Figure 17c,d).

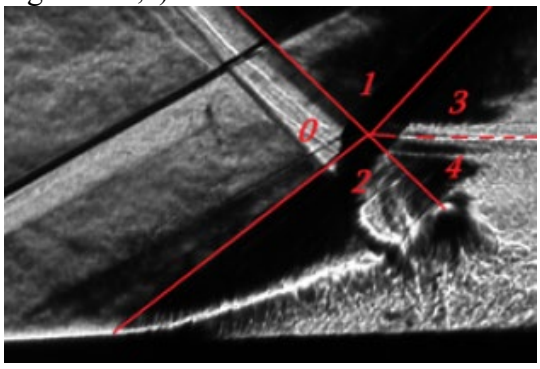

a) Spark light Schlieren visualization – regular reflection

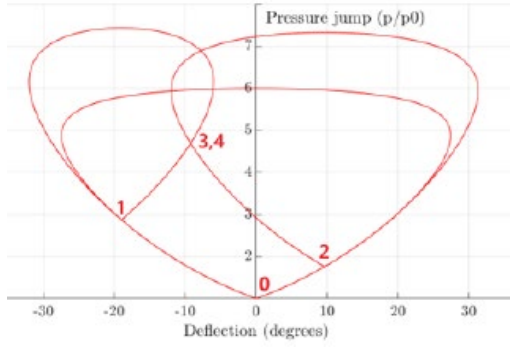

b) Shock polar – regular reflection

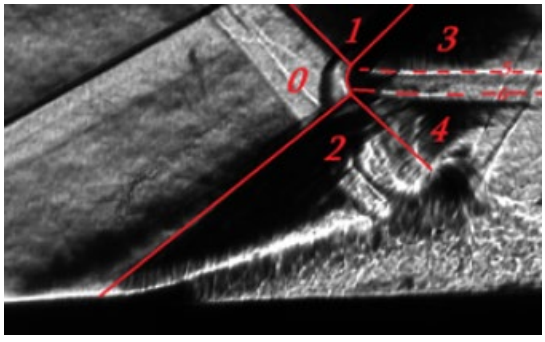

c) Spark light Schlieren visualization – Mach reflection

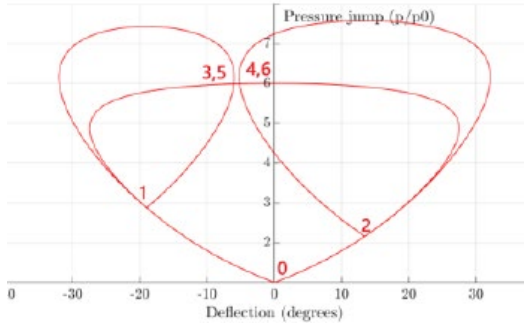

d) Shock polar – Mach reflection

Figure 17. Dual domain appearing in a case with a "desired oscillation"

Taken together, these results showed that the baseline case exhibits the transitional OSBLI features central to this study: a well-defined low-frequency oscillation, a Reynolds number consistent with early transition, and the intermittent appearance and disappearance of a Mach stem. This combination of frequency analysis and shock-polar diagnostics demonstrates the inherently unsteady and multi-regime nature of strongly separated transitional OSBLIs. Following the baseline analysis, the same methodology was applied to all selected test cases from Table 1.

Each case was examined by visually inspecting the Schlieren recordings to track the motion of the laminar separation shock, measuring how far upstream it propagated before vanishing, and by analyzing the associated FFT/PSD spectra.

Angle measurements of the separation and reflected shocks were used to construct shock polars, enabling classification of the interaction as either regular or Mach reflection. These steps allowed direct comparisons to be drawn between each test case and the baseline reference,

clarifying the influence of Mach number, Reynolds number, and shock generator angle on the oscillatory behavior of transitional OSBLIs.

From these analyses, several preliminary observations emerged. The presence of a "dual" domain (marked by the constant shift between Mach reflection and regular reflection) was consistently associated with cases where the desired oscillation appeared clearly. When only Mach reflection persisted throughout the interaction, faint low-frequency peaks were still observed in the PSD, but the oscillation amplitude and upstream shock travel length were significantly smaller.

Conversely, cases where only a regular reflection was present showed almost no discernible low-frequency peaks, and no distinct oscillation mechanism could be confirmed.

These findings are summarized in Table 2, which highlights the correlation between reflection type, transitional Reynolds-number conditions, and the presence or absence of the oscillation.

Table 2. Summary of the observations from the test cases analyzed

No.	**Shock generator**	***Re*$_x$ within transitional range (Giepman, 2016)?**	**Mach reflection observed?**	**Oscillation mechanism observed**
1	19°	Yes	Appearing and disappearing	Desired oscillation
2	19°	Yes	Only Mach reflection	Desired oscillation faintly observed
3	19°	Yes	Only Mach reflection	Desired oscillation faintly observed
4	19°	No	Only Mach reflection	Desired oscillation not observed
5	19°	Yes	Regular reflection mostly observed	Desired oscillation very faintly observed
6	19°	Yes	Only regular reflection	Desired oscillation not observed
7	19°	Yes	Only regular reflection	Desired oscillation not observed
8	17°	Yes	Appearing and disappearing	Desired oscillation
9	17°	Yes	Regular reflection mostly observed	Desired oscillation very faintly observed
10	22°	Yes	Appearing and disappearing	Desired oscillation
11	22°	Yes	Only Mach reflection	Desired oscillation faintly observed
12	22°	Yes	Only regular reflection	Desired oscillation not observed
13	22°	Yes	Only regular reflection	Desired oscillation not observed

The frequency analyses across all shock generator angles confirmed these trends. For each angle (17°, 19°, 22°), the clearest PSD peaks were observed in the cases where the "dual" domain occurred, while weaker peaks corresponded to permanent Mach reflections and no peaks to permanent regular reflections.

To better illustrate this, only the relevant cases with observable unsteadiness were retained and compared (Figure 18).

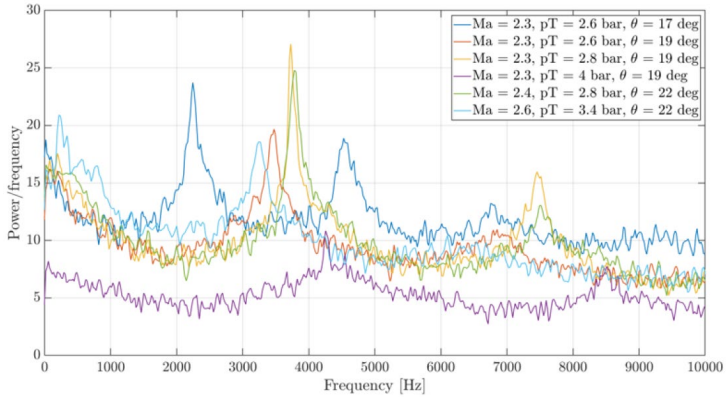

Figure 18. Frequency content of all test cases where the desired oscillation mechanism is at least "faintly" observed

The result confirms that the strongest low-frequency content coincides with the alternating appearance and disappearance of the Mach stem, underscoring its role as a key feature of the oscillation mechanism in highly separated transitional OSBLIs.

Addition of the 2D step

To evaluate the effect of passive flow control, thin 2D steps of varying heights were applied to the flat plate. Schlieren snapshots comparing the undisturbed baseline with cases including 60, 120, and 180 μm steps (Figure 19) clearly demonstrate that even the smallest step height alters the interaction significantly. With one layer applied (Figure 19a), the oscillation amplitude of both the separation and reflected shocks was already reduced, and the upstream excursion of the laminar separation shock nearly vanished. Increasing the step height further dampened the dynamics, with the interaction shifting away from transitional OSBLI behavior.

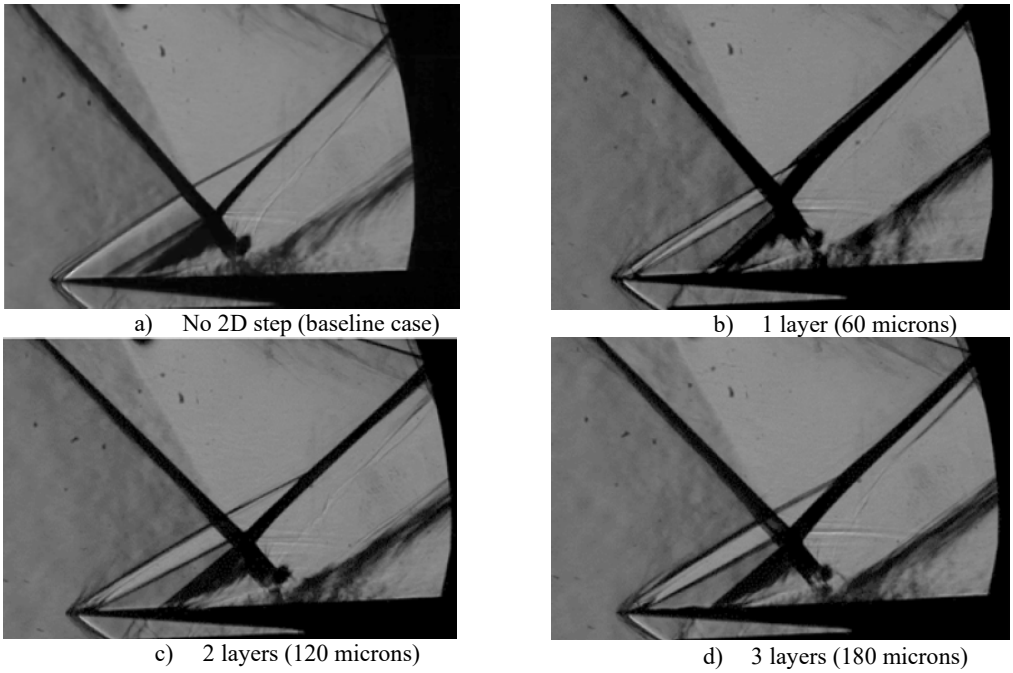

a) No 2D step (baseline case) b) 1 layer (60 microns)

c) 2 layers (120 microns) d) 3 layers (180 microns)

Figure 19. Shock travel comparison with 2D step - reference case (Ma = 2.3, pT = 2.8 bar, 19º shock generator)

These visual observations are confirmed by the frequency analysis (Figure 20). While the undisturbed baseline displayed a distinct low-frequency peak associated with the shock breathing mechanism (Figure 20a), this peak disappeared completely once a 60 μm step was introduced (Figure 20b). The trend persisted with additional step layers, where no clear oscillation frequencies were detected in the PSD. Thus, even minimal boundary-layer tripping was sufficient to suppress the unsteady separation–shock system and eliminate the dual-domain oscillation mechanism.

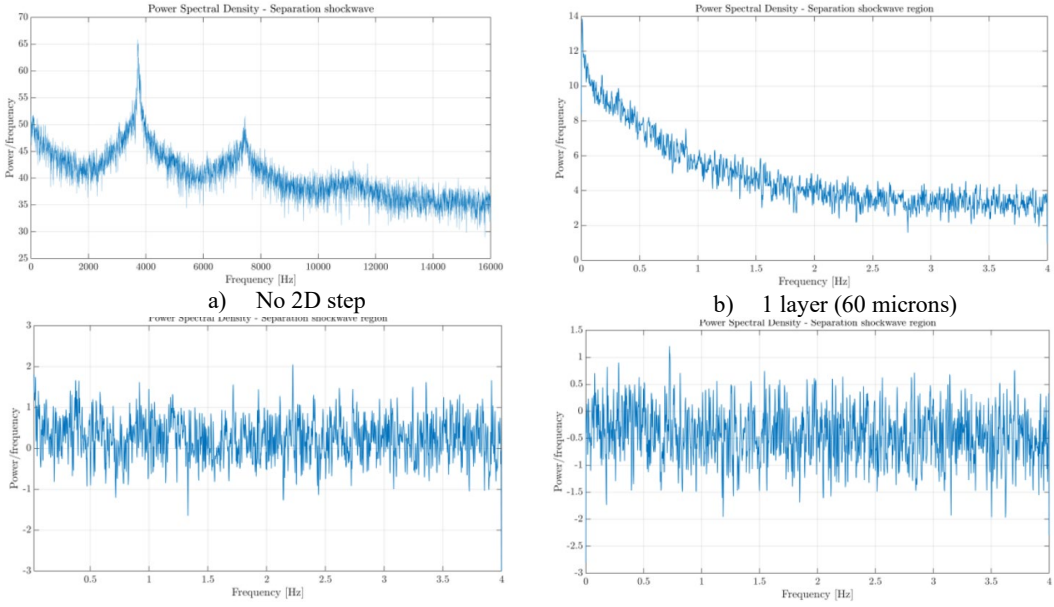

a) No 2D step b) 1 layer (60 microns)

c) 2 layers (120 microns) d) 3 layers (180 microns)

Figure 20. Frequency content comparison with 2D step - reference case (Ma = 2.3, pT = 2.8 bar, 19° shock generator)

Taken together, these results highlight the sensitivity of transitional OSBLIs to boundary-layer disturbances. The introduction of a small artificial step effectively stabilized the flow by preventing the upstream motion of the separation shock and disrupting the conditions necessary for low-frequency oscillations. This confirms that passive tripping can strongly alter the state of the interaction, shifting it away from the transitional regime central to the unsteady behavior investigated in this study.

Nondimensional analysis

To complement the raw frequency comparisons, the oscillatory behavior of the interaction was further investigated using the Strouhal number, defined as:

$$\mathrm{St} = \frac{fL}{U} \tag{5}$$

where f is the dominant frequency, L a characteristic length, and U the freestream velocity (Eq. 5). The choice of length scale is critical, and two options were considered (Figure 21): the laminar separation shock travel length (L_{12}) and the interaction length (L_{13}), the latter being the classical scaling parameter for OSBLI analyses [12].
Since both have been applied in prior studies, including Nel et al. [4], both definitions were retained for the present comparison.

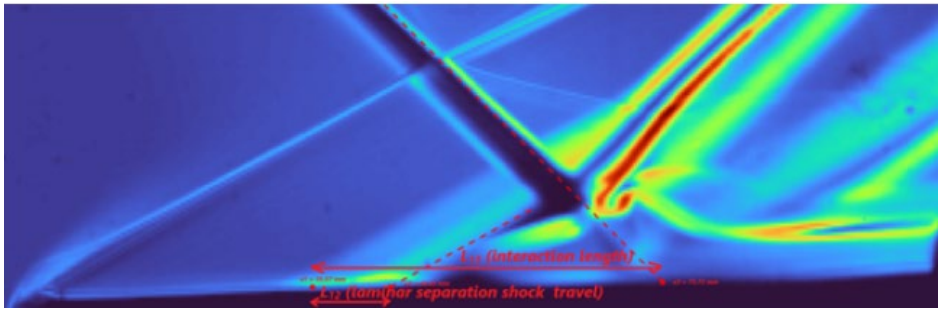

Figure 21. Length scales that can be used in the non-dimensional analysis

Focusing only on cases where the oscillation mechanism was clearly observed, the Strouhal analysis revealed a notable collapse around a value of 0.33. Table 3 summarizes the main cases.

Table 3. Nondimensional comparison of all cases where the oscillation is observed

No.	p_T [bar]	*Ma*	Shock generator	Re_x [million]	L_{13} (length of the interaction) [mm]	U [m/s]	Dominant frequency [Hz]	St_{13} (based on L_{13})
1	2.3	2.6	17°	2.22	40.15	545	4529	0.33
2	2.3	2.6	19°	2.01	46.6	545	3475	0.3
3	2.3	2.8	19°	2.06	48.45	545	3728	0.33
4	2.3	4	19°	2.97	44.7	545	4256	0.35
5	2.4	2.8	22°	1.9	50	557	3800	0.33
6	2.6	3.4	22°	2.41	58	577	3270	0.32

Figure 22 shows that, although the raw frequencies varied from case to case, the corresponding Strouhal numbers consistently collapsed near this preferred value. Most importantly, the three cases identified as exhibiting the "desired oscillation" with higher amplitude and clearer unsteadiness all shared an identical Strouhal number of 0.33. This consistency suggests the presence of a fundamental nondimensional scaling for transitional OSBLIs, with the Strouhal number offering a reliable parameter for cross-comparison across different flow conditions.

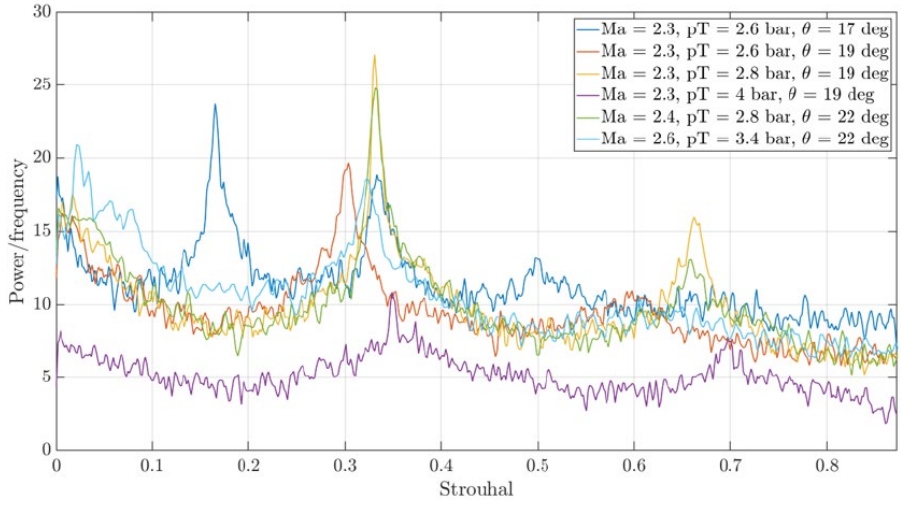

Figure 22. Strouhal number comparison

The influence of the Reynolds number was examined separately using cases at constant Mach number and shock generator angle, but with varied total pressures. Table 4 compiles these results, which show a clear trend: increasing Reynolds number reduced the laminar separation

bubble length and increased the dominant oscillation frequency. This effect is consistent with the expectation that higher Reynolds numbers promote earlier transition, thus shortening the distance over which the laminar separation shockwave can travel upstream. The Strouhal numbers derived from the interaction length also followed this trend, confirming that higher Re_x values correspond to faster oscillatory behavior.

Table 4. Strouhal number comparison

No.	p_T [bar]	Re_x [million]	L_{13} (interaction length) [mm]	L_{12} (laminar separation bubble length) [mm]	U [m/s]	Dominant frequency [Hz]	St_{13}	St_{12}
1	2.6	2.01	46.6	11.4	545	3475	0.3	0.073
2	2.8	2.06	48.45	10.34	545	3728	0.33	0.07
3	4.0	2.97	44.7	8.54	545	4256	0.35	0.067

In summary, the non-dimensional analysis demonstrated that transitional OSBLIs with a clear oscillation mechanism collapse to a Strouhal number of approximately 0.33, with the dual-domain behavior always present in these cases. Increasing Reynolds number shifted the oscillation toward higher frequencies and reduced the shock excursion amplitude, fully consistent with theoretical expectations of boundary-layer transition effects.

8. CONCLUSIONS

This study investigated the mechanisms driving low-frequency unsteadiness in highly separated transitional OSBLIs. It was shown that Mach number, Reynolds number, inviscid pressure jump, and the occurrence of a dual-domain structure dictate the oscillation behavior. A strong correlation was found between the appearance/disappearance of a Mach stem and the presence of low-frequency instabilities, though this mechanism alone was not proven to be either necessary or sufficient. The transitional Reynolds number regime identified by Giepman [10] was confirmed, with laminar separation followed by accelerated transition leading to significant changes in oscillation amplitude and frequency. Passive control experiments further revealed that even minimal 2D step heights (~60 μm) were sufficient to suppress the oscillatory mechanism entirely.

The non-dimensional analysis provided a consistent collapse of results at a Strouhal number of approximately 0.33 across all cases where the “desired oscillation” was observed. Despite different raw frequencies, the unsteadiness scaled reliably with the interaction length and free-stream velocity, establishing this Strouhal number as a fundamental parameter for transitional OSBLIs. An increase in the Reynolds number was associated with shorter laminar separation shock excursions and higher oscillation frequencies, consistent with faster boundary-layer transition. Together, these findings highlight the delicate balance of parameters governing transitional shock–boundary layer interactions.

Future research should aim to extend the current findings by overcoming tunnel limitations to allow broader parametric studies at constant Reynolds number while varying shock strength. Automated shock-tracking tools and predictive models for separation bubble dynamics would improve accuracy and planning. Addressing three-dimensional interference effects, particularly from expansion waves at the shock generator shoulder, would refine the interpretation of 2D configurations. Finally, combining Schlieren with complementary techniques such as PIV, oil-flow visualization, and CFD would yield more detailed insights into boundary-layer development and provide validation for the experimental database.

ACKNOWLEDGMENT

The first author of this article was awarded The **"Caius IACOB"** Prize at the "Awards Gala" of the *41st "Caius IACOB" Conference on Fluid Mechanics and its Technical Applications, held on 30 - 31 October, 2025*, at the headquarters of the INCAS, Blvd. Iuliu Maniu 220, sector 6, Bucharest, Romania.

REFERENCES

[1] H. Babinsky and J. Harvey, "*Shock Wave-Boundary Layer Interactions*," Cambridge University Press, 2011.

[2] J. Watts, "*Flight experience with shock impingement and interference heating on the x-15-2 research airplane*," NASA, Tech. Rep. TM X-1669, 1968.

[3] P. Doerffer, P. Flaszynski and J.-P. Dussauge, *Transition Location Effect on Shock Wave Boundary Layer Interaction*, Experimental and Numerical Findings from the TFAST Project, Springer, 2021.

[4] P. Nel, A.-M. Schreyer, F. Schrijer, B. van Oudheusden, C. Janke and M. Swoboda, "*Research configuration to study shock oscillation mechanisms*," 2024.

[5] J. Denton, "The effects of lean and sweep on transonic fan performance: A computational study," *Cambridge University Engineering Department, Cambridge, Tech. Rep.,* 2022.

[6] P. Nel, A.-M. Schreyer, F. Schrijer and B. van Oudheusden, "*Shock oscillation mechanism of highly separated transitional shock-wave/boundary layer interactions*," 2024.

[7] P. Nel, C. Janke and I. Vasilopoulos, "Effect of transition on self-sustained shock oscillations in highly loaded transonic rotors," *AIAA Journal,* 2024.

[8] D. Chapman, D. Kuehn and H. Larson, "*Investigation of separated flows in supersonic and subsonic streams with emphasis on the effect of transition*," NACA, Tech. Rep. Report No. 1356, 1957.

[9] J. Erdos and A. Pallone, "Shock-boundary layer interaction and flow separations," *Proceedings of the 1962 Heat Transfer and Fluid Mechanics Institute,* 1963.

[10] R. Giepman, "Flow control for oblique shock wave reflections," *Ph.D. dissertation, Technical University of Delft,* 2016.

[11] D. Dolling, "Fifty years of shock-wave/boundary-layer interaction research:What next?," *AIAA Journal,* vol. **39**, no. 8, 2001.

[12] J.-P. Dussauge, P. Dupont and J.-F. Debieve, "Unsteadiness in shock wave boundary layer interactions," *Aerospace Science and Technology,* vol. **10**, pp. 85-91, 2006.

[13] G. Ben-Dor, O. Igra and T. Elperin, *Handbook of ShockWaves*, Three Volume Set, Beer Sheva: Elsevier Science, 2001.

[14] N. Sandham, E. Schuelein, A. Wagner, S. Willems and J. Steelant, "Transitional shock-wave/boundary-layer interactions in hypersonic flow, "*Journal of Fluid Mechanics*", vol. **752**, pp. 349-382, 2014.

[15] V. Pasquariello, M. Grilli, S. Hickel and N. Adams, "Large-eddy simulation of passive shock-wave/boundary-layer interaction control, "*International Journal of Heat and Fluid Flow*", vol. **2014**, pp. 116-127, 2014.